 doi:10.20944/preprints202105.0077.v1

Article

Imaging the morphological structure of silk fibroin constructs through fluorescence energy transfer and confocal imaging

Alessio Bucciarelli [1,*], Alberto Quaranta[2] and Devid Maniglio[3]

[1] CNR Nanotech, Institute for nanotechnology, National Council of Research, via Monteroni, 73100 Lecce, Italy.
[2] Department of Industrial Engineering, University of Trento, Via Sommarive 9, 38123 Trento, Italy.
[3] BIOtech Research Center, Department of Industrial Engineering, University of Trento, Via delle regole 18, 38123 Trento, Italy.
* Correspondence: Alessio.bucciarelli@nanotec.cnr.it;

Abstract: Silk fibroin is a well-known biopolymer used in several applications in which the interaction with biological tissue is required. In fact, fibroin is extremely versatile and can be shaped to form several constructs useful in tissue engineering applications. Confocal imaging is usually performed to test the cells behaviour on the construct and in this context the fibroin intrinsic fluorescence is regarded as a problem. In addition, the intrinsic fluorescence is not intense enough to provide useful morphological images. In fact, to control study the constructs morphology other techniques are used (i.e. SEM, Micro-CT). In this work we propose a method based on the fluorescence energy transfer (FRET) to suppress the fibroin intrinsic fluorescence moving it to higher wavelength accessible to the confocal microscopy for a direct imaging.

Keywords: Silk Fibroin, Fluorescence Resonance Energy Transfer (FRET), Confocal Imaging, Electrospinning.

1. Introduction

Silk Fibroin is the internal protein of the silk fiber and is the main responsible for its mechanical strength. Fibroin possesses several interesting properties, an incredibly high mechanical strength, an excellent biocompatibility, a high transparency when used as films. In addition, among other biopolymers (i.e. keratin [1], chitosan[2], alginate[3], gelatin [4]) is extremely versatile and can be used to prepare a vast variety of materials [5,6]. Fibroin founds its main applications in Tissue Engineering [7,8] as source for the development of scaffolds [9–11], and, in recent years, in frontiers applications encountering other disciplines as in the case of bio-electronics [12] and in bio-optics [13,14]. The morphological analysis of silk fibroin constructs is usually obtained using imaging techniques as secondary electron microscopy (SEM), micro-computer tomography (micro-CT) and optical microscopy. In few cases also fluorescence microscopy and confocal microscopy have been used by dissolving specific fluorophore and observing their emission when excited at their specific excitation wavelength [15]. Silk fibroin possesses its own fluorescence emission due to both the presence of the aromatic structures of two amino acids, tryptophane and tyrosine and to the mutual interaction of their excitation-emission profiles [16]. This emission, is also known to be dependent on the conformation of the secondary structure of the protein [16]. The fibroin intrinsic fluorescence has been always regarded as problematic because of its low intensity and that do not allow to effectively visualize the fibroin structure and the wide emission that still consent to interfere with the emission of some typical staining for cells imaging [17]. For these reasons a method able to suppress the fibroin emission moving it to longer wavelength, where the morphological structure of fibroin can be effectively visualized by confocal is desirable.

 doi:10.20944/preprints202105.0077.v1

Fluorescence Resonance Energy Transfer (or Förster Resonance Energy Transfer, FRET) is a physical phenomenon first described for the first time almost 50 years ago and describe a mechanism of energy transfer between two light sensitive molecules that occurs through a non-radiative dipole-dipole coupling [18]. The two molecules are usually referred as donor and acceptor. The donor is the molecule that initially absorbs the energy while the acceptor is the molecule to which the energy is subsequently transferred. This resonance interaction occurs on a higher scale than the interatomic distances, without conversion to thermal energy, and without any molecular collision [18]. The transfer of energy leads to a reduction in the donor's fluorescence intensity and excited state lifetime, and an increase in the acceptor's emission intensity. A pair of molecules that interact in such a manner that FRET occurs is often referred to as a donor/acceptor pair. While there are many factors that influence FRET, two needs to be met in order to allow the energy transfer. The absorption or excitation spectrum of the acceptor must overlap the fluorescence emission spectrum of the donor and the distance between the donor and the acceptor should be small enough to allows the molecules to interact. In fact, FRET is highly efficient if the donor and acceptor are positioned within the Förster radius (the distance at which half the excitation energy of the donor is transferred to the acceptor), typically 3–6 nm [19]. The efficiency of FRET is inversely proportional to the sixth power of the distance between donor and acceptor making it extremely sensitive to the change of distance. The fluorescence intensity is then related to the distance and FRET can be used accurate measurement method of molecular proximity at angstrom distances (10–100 Å). This principle has been used also to develop the FRET microscopy that apply the principle of the energy transfer in confocal microscopy to capture fluorescent signals from the interactions of molecules labeled with the fluorophore [20]. However, this technique has been limited to the understanding of molecular interaction in cells.

In this work we demonstrated the possibility of using FRET to shift the silk fibroin intrinsic fluorescence emission towards longer wavelength and then by confocal microscopy to study the morphology on a silk construct. This has been done by creating a silk fibroin matrix incorporating two fluorophore, 2,5-diphenyloxazole (PPO) and Lumogen F Violet 570, both organic dyes used in different applications from probing [21,22] to solar cells [23]. This couple of fluorophores have been used in other studies as energy transfer system to move the fluorescence emission at longer wavelength [24]. Initially, to understand if the energy transfer occurred between silk fibroin and PPO, we studied fibroin films with increased concentration of PPO. We collected the entire excitation-emission space, but the optimal sample was selected by exiting silk fibroin at 290 nm and observing the emission spectra. On the optima Fibroin-PPO composition we added an increasing amount of LV producing a second set of films to find the best composition. Finally, as proof of concept we produced by electrospinning three mats (the pure protein, the optimized formulation with PPO, the optimized formulation with PPO and LV), that were observed by confocal microscopy to study their morphology. As results we were able to better observe and study the morphology when both fluorophores were present, avoiding excessive increase of the laser intensity and photomultiplier gain.

2. Materials and Methods

2.1. Silk Fibroin Degumming

Degummed silk fibroin has been obtained by a modified version of a well-established protocol [5,6]. Briefly the cocoons (imported from Chul Thai Silk Co., Phetchabun, Thailand) were cut in pieces and placed in a 0.01M hot bath of sodium carbonate (Na_2CO_3, Sigma-Aldrich) for 1h, followed by a second immersion in a bath with a concentration of 0.003M for 1 h. The resultant silk fibroin (SF), progressively taken at room temperature, was carefully rinsed for three times using ultra-pure water and then dried for 2d. The resulting degummed silk fibroin was dissolved into a 9.3M water solution of lithium bromide (Sigma-Aldrich) at 60 °C for 4 h in a concentration of 2g/10mL. Once SF was dissolved the solution was taken at room temperature and then dialyzed against water for 3d in a dialysis tube (cutting Mw = 3kDa) to remove the salt. The solu-

Preprints (www.preprints.org) | NOT PEER-REVIEWED | Posted: 6 May 2021 doi:10.20944/preprints202105.0077.v1

tion was frozen into 50 mL vials by the use of liquid nitrogen and then lyophilized in at -50°C until the complete removal of the water.

2.2. Praparation of the solution and fluorescent fibroin films

The emission and absorption of the pure fluorophore were tested in Formic Acid solution by preparing a 10^{-5}M solution (the concentration has been chosen to not saturate the emission).

To prepare the films with PPO a known amount of lyophilized SF has been dissolved in Formic Acid in a ratio of 100mg/mL, then a predetermined amount of 2,5-diphenyloxazole (PPO, Sigma Aldrich, 0.01%, 0.1% and 1% w/w) has been added to the solution and mixed until clear. The films were formed by drop casting, 2mL of solution were deposited into a 3 cm petri dish and leaved to evaporate under the hood. The same procedure has been performed for the addition of the Lumogen Violet (LV, Basf), but a single concentration of PPO has been selected (1% w/w) while LV has been added with in different concentrations (0.01%, 0.03%, 0.04%). On this trial the best compositions have been chosen.

2.3. Preparation of silk fibroin mats by elecrospinning

Similarly to what done for films casting, a mother solution composed of 10% v/w fibroin in formic acid was prepared for electrospinning. Two different solutions where then derived: the first one obtained by adding PPO and the second one by adding PPO and LV (1% w/w and 0.2% w/w with respecto to the fibroin weight, respectively). The three solutions were then loaded in 5mL plastic syringes mounting a 22 Gauge needle. Electrospinning was obtained extruding the solutions (fibroin, fibroin + PPO, fibroin + PPO + LV) through the syringe by means of a motorized piston to keep the flow rate constant (0.250 mL/h), and applying a voltage potential of 15 kV to the needle. An aluminum foil set at groud potential and positioned at 12 cm from the needle tip, was used as collector electrode.

2.4. Characterization

The absorption of the pure fluorophore in FA solution were tested by Jasco VR-570 UV–Vis spectrophotometer, while the emission with a tested by a Jasco FP-6300 spectrofluorometer using the wavelength of the maximum absorption.

The fluorescence 3D spectra were acquired with a Jasco FP-6300 spectrofluorometer. The bare fibroin film and the films with PPO where between 250 nm and 320 nm and the emission was collected the emission between 270 nm and 450 nm. The films samples with the addition of LV where excited between 250 nm and 500 nm and the emission was collected the emission between 300nm and 550nm. The 3D emission spectrum was done by collecting an emission spectrum at a specified excitation wavelength then moving the excitation wavelength of 10 nm and collecting the emission again. All the samples were placed at 45◦ inside the chamber. The contour plot was reconstructed by R [25] within the plotly library [26].

Laser Scanning confocal microscopy was performed on the electrospun networks using a Nikon A1 confocal microscope. A 504 nm wavelength laser was used fluorescence excitation while emission was collected wither using a spectral detector to reconstruct the emission spectrum with a 6 nm amplitude channel, for a total of 32 channels spanning the range 405-596 nm. To permit spectra comparison, pinhole aperture, laser intensity and amplifier gain were set constant for all the samplings.

For better sensitivity, a high resolution and low noise confocal microcopy picture of PPO+LV containing network was collected through a 450/50 nm band-pass filter and a PMT photodetector.

An image analysis was conducted by ImageJ [27], the intensity profile of 70 fibers was evaluated and the diameter extrapolated.

Preprints (www.preprints.org) | NOT PEER-REVIEWED | Posted: 6 May 2021 doi:10.20944/preprints202105.0077.v1

3. Results

3.1. Emission spectra

Two amino acids structures responsible for the intrinsic fluorescence of silk fibroin are shown in **Figure 1A** (tryptophane) and **1B** (Tyrosine), while the structure of the fluorophore used are reported in Figure **1C** (PPO) and **1D** (LV). The absorption spectra superimposed to the emission of the two fluorophores are reported in **Figure 1E**. The superposition of the emission spectrum of PPO and the absorbance spectrum of LV allowed an efficient energy transfer from these two fluorophores.

The combined effect of tryptophane and tyrosine resulted in an absorption that had its maximum at 290nm with an emission centered at 330nm, as reported in **Figure 2A** in the 3D fluorescence contour plot of pure fibroin. With the increasing in the percentage of added PPO the emission of fibroin was progressively suppressed while the fluorescence emission of PPO increased to a point in which the emission of fibroin not visible and only the large PPO emission peak was present with two maxima centered at 370nm and 380nm. This effect was better observed by slicing the surfaces at 290nm excitation (red lines in **Figure 2A**-**2D**) and plotting the emission (**Figure 2E**) where the clear effect is the reduction of the Fibroin emission and a contemporary increase in the PPO emission. The best result was obtained by the addition of 1% of PPO, on this formulation we added the LV in an increasing concentration (0.02%, 0.03% and 0.04% respect to the weight of the dissolved fibroin), the results are shown in **Figure 3.** In this case the trend resulted to be in countertendency respect to the one shown by the fibroin-PPO couple. In fact, with the increasing in amount of LV the energy transfer seems to be less efficient (moving from **Figure 3A** to **Figure 3B** and **3C**). This effect results even more evident by slicing the fluorescence surfaces (**Figure 3A**-**3C**) along the excitation at 290nm (red lines). The result is shown in **Figure 3E**, whit the increment in the LV percentage the emission of PPO increased, and the emission of LV decreased.

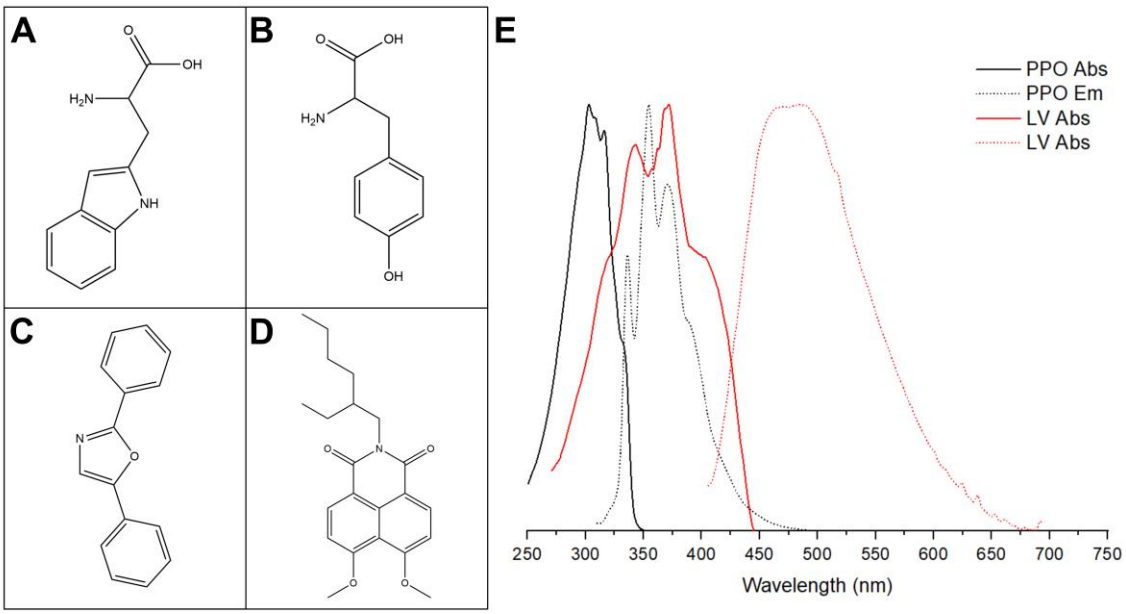

Figure 1. Chemical structure of (A**)** Tryptophan, (B) Tyrosine, (C) 2,5-diphenyloxazole (PPO), and (D) Lumogen F Violet. (E) The absorption and emission spectra of the used fluorophore within the local maxima. How can be clearly seen the emission of PPO falls inside the absorption of LV. This allows to excite the first and observe the emission of the second if the distance between the donor (PPO) and the acceptor (LV) is small enough.

Preprints (www.preprints.org) | NOT PEER-REVIEWED | Posted: 6 May 2021 doi:10.20944/preprints202105.0077.v1

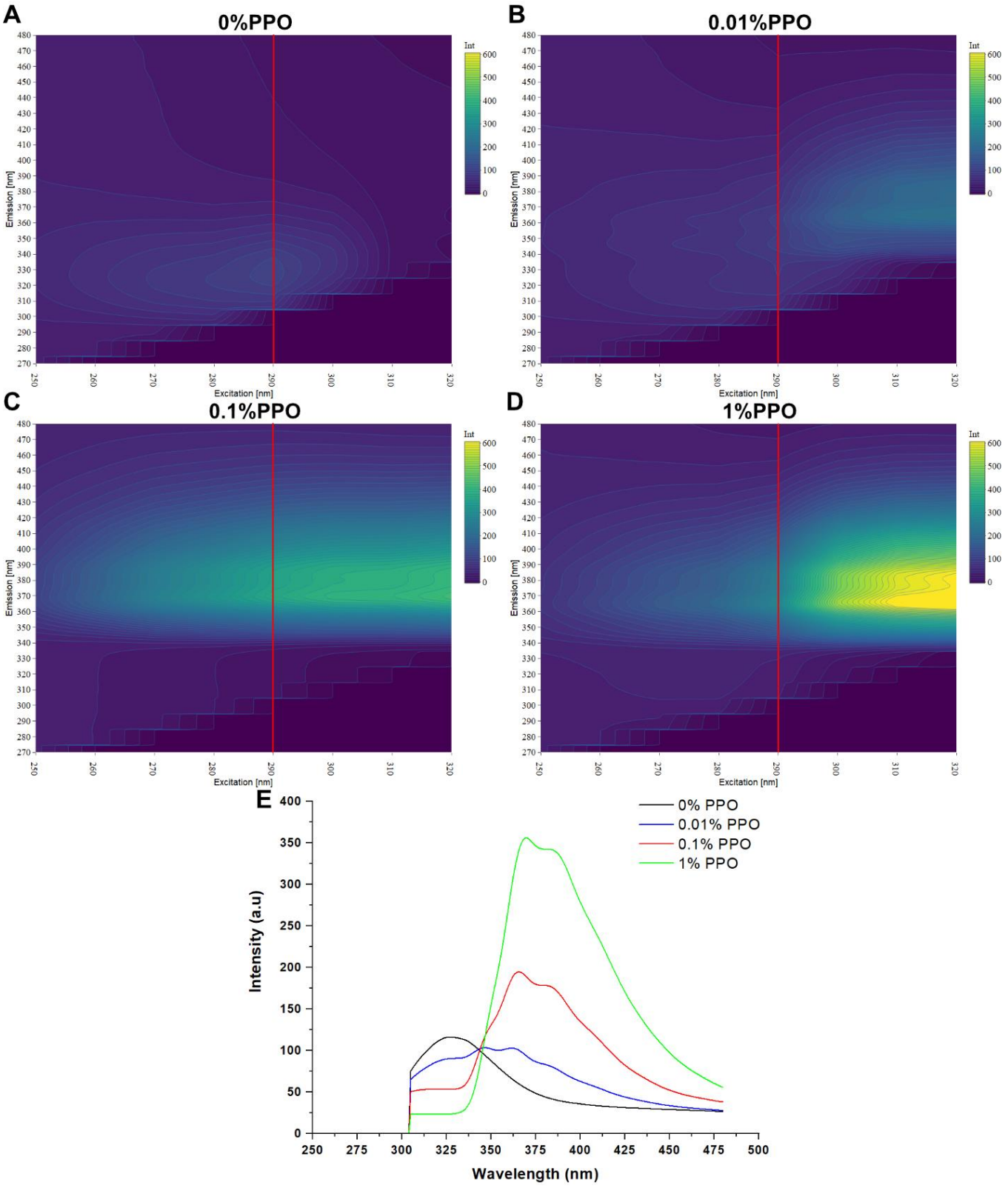

Figure 2. Fluorescence contour plot of the (A) bare silk fibroin, (B) silk fibroin with the addition of 0.01% of PPO, (C) silk fibroin with the addition of 0.1% of PPO and (D) silk fibroin with the addition of 1% of PPO. (E) Slicing of the fluorescence contour plot at the excitation wavelength of 290nm. The emission was truncated at 305 nm to cut out the wavelength at which the films were exited (290 nm).

3.2. Confocal Imaging

Preprints (www.preprints.org) | NOT PEER-REVIEWED | Posted: 6 May 2021 doi:10.20944/preprints202105.0077.v1

The confocal study of the prepared samples is shown in **Figure 4.** Three samples were analyzed, a film produced by the bare protein (**Figure 4B**, **4C**), one produced with the addition of 1% w/w of PPO and the last with the addition of 1% of PPO (**Figure 5D**, **4E**) and 0.02% of LV (**Figure 4F**, **4G**, **4H**). We collected one image for each channel for each sample. In this way we were able to evaluate the fluorescence emission (**Figure 4A**) at different wavelength. The best result in term of resolution was obtained from the sample obtained by the addition of both PPO and LV selecting the 447nm-452nm channel (**Figure 4F**). In fact, in that condition the fibers resulted to be well recognizable. In the same condition neither the fibroin sample (Figure 5B) nor the sample with PPO (Figure 5D) gave an acceptable result even if in the case of the addition of PPO some of the fibrous structures of the mats was visible. By combining all the channel in a single image, the trend among the samples remained the same (as visible in **Figure 4C**, **4E** and **4G**).

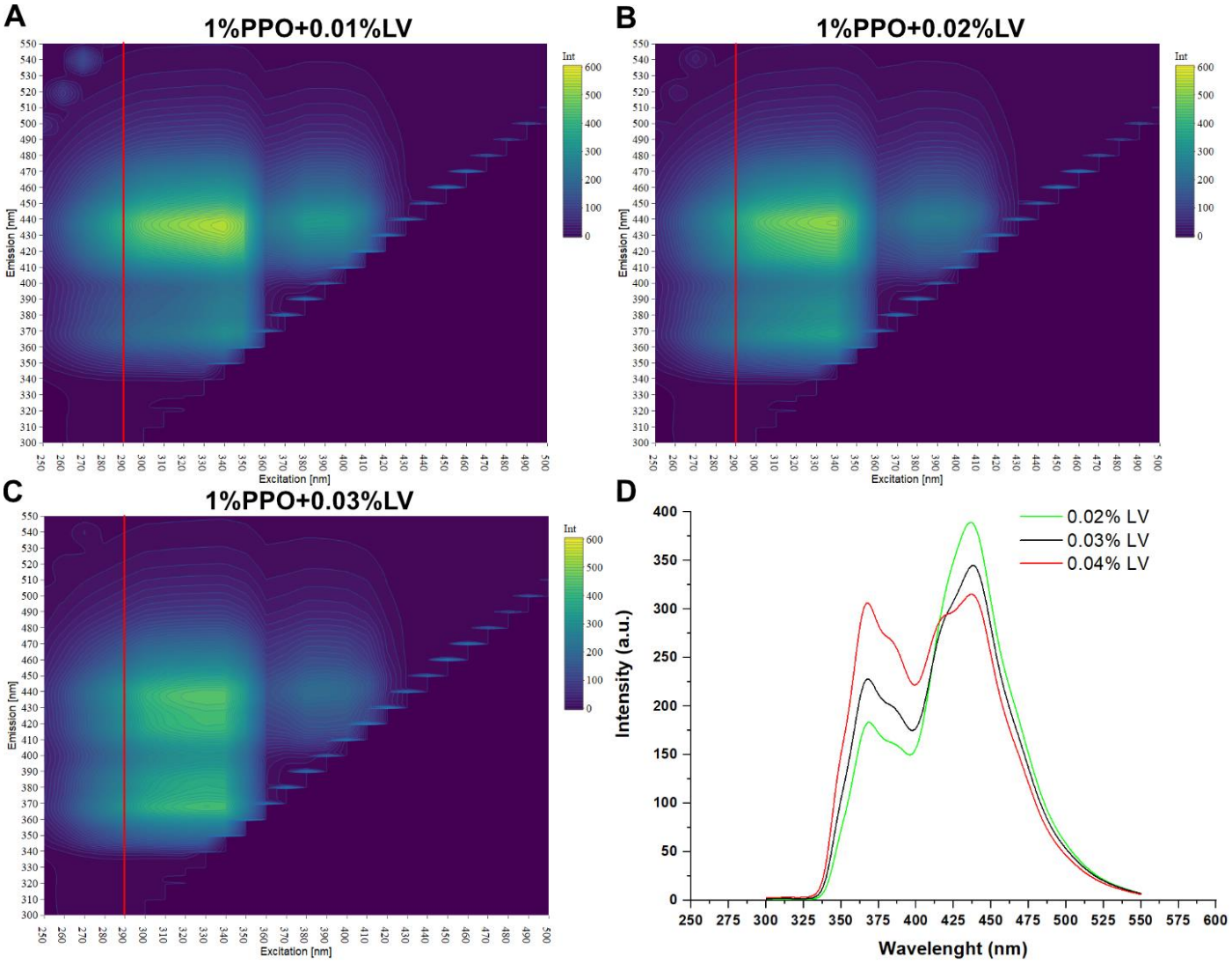

Figure 3. Fluorescence contour plot of the (A) bare silk fibroin with 0.1% of PPO, (B) silk fibroin with the addition of 0.1% of PPO and 0.02% of LV, (C) silk fibroin with the addition of 0.1% of PPO and 0.03% of LV and (D) silk fibroin with the addition of 0.1% of PPO and 0.04% of LV. (E) Slicing of the fluorescence contour plot at the excitation wavelength of 290nm.

By the use of a photomultiplier the image presented in **Figure 5E** was produced to maximize the resolution of a single slice in the z-stack. The result clearly shown the single fibers that are well distinguishable. From that image we were able to determine the fiber diameter distribution shown in **Figure 4I**. The distribution resulted to be skewed towards

Preprints (www.preprints.org) | NOT PEER-REVIEWED | Posted: 6 May 2021 doi:10.20944/preprints202105.0077.v1

the lower dimeter values and well fitted by a log-normal function with a maximum at 0.54μm and a standard deviation (SD) of 0.32 μm (red curve). It should be noticed that in this case the standard deviation should be regarded as a measure of the distribution width. On the distribution we also calculated the descriptive statistic, the mean value and the corresponding SD resulted to be 0.61μm and 0.22μm, respectively, while the median and the corresponding interquartile range (IQR) resulted to be 0.55μm and 0.26μm, respectively. It should be noticed that for a skewed distribution, as in our case, the median and the IQR are the correct statical descriptor. In addition, those value resulted to be in accordance with the one calculated by the lognormal fitting.

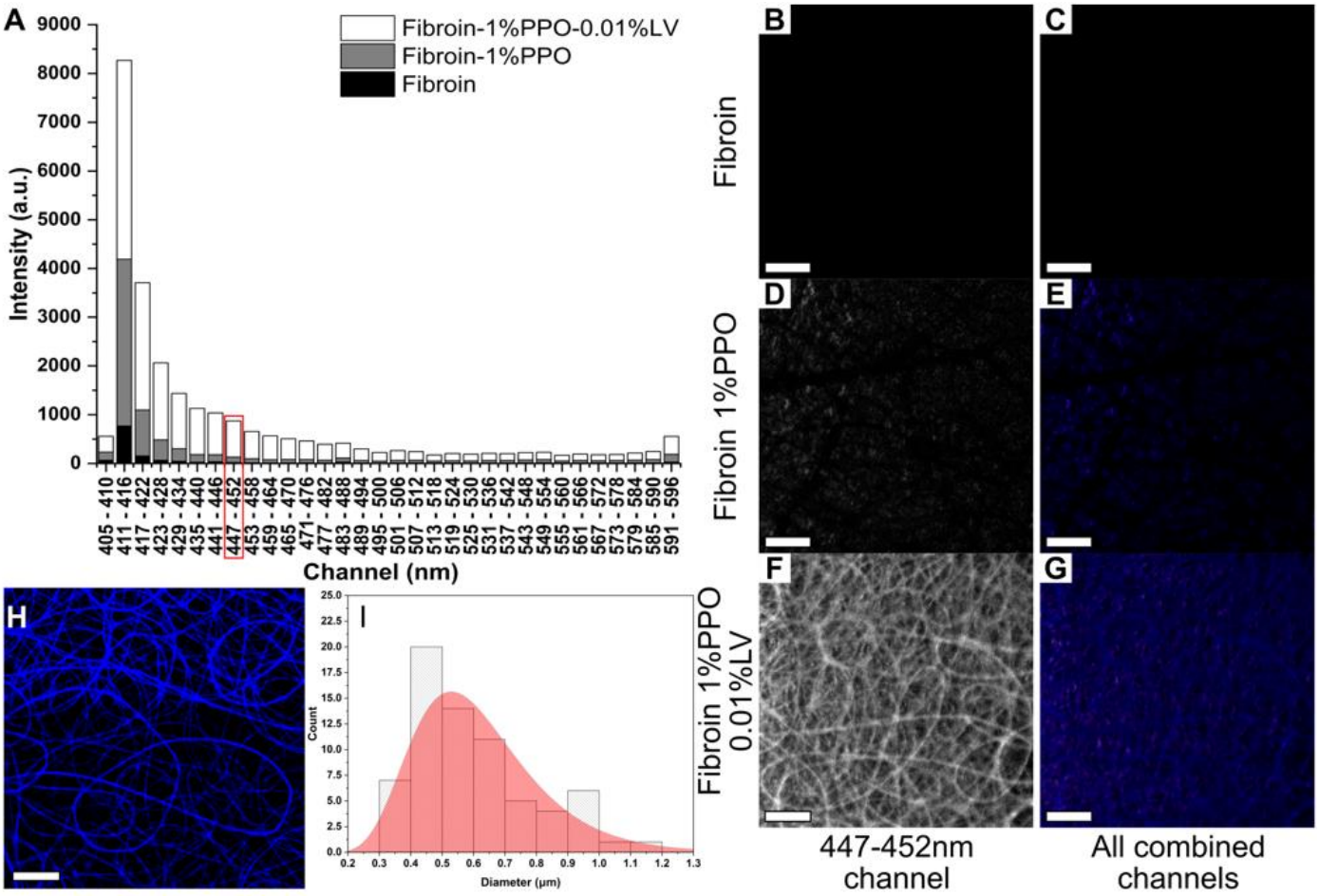

Figure 4. Confocal study on silk fibroin mats produced by electrospinning. (A) Fluorescence emission for the collected image divided in 32 emission channels (bandwidth od 5nm). Images collected in the 447-452 channel for (B) the bare fibroin, (D) fibroin with 1% of PPO and (F) Fibroin with 1% of PPO and 0.01% of LV. Images of all the combined channels with adjusted intensities for (C) the bare fibroin, (E) fibroin with 1% of PPO and (G) Fibroin with 1% of PPO and 0.01% of LV. (H) Hi-Res Image collected by the photomultiplier in for the sample prepared with 1% of PPO and 0.01% of LV. All the scale bars are 20μm. (I) Diameter distribution calculated on the Hi-Res image.

4. Discussion

A general scheme of the principle of how this phenomenon worked in our samples is shown in **Figure 5**. Silk fibroin is constituted of two domains. The heavy chain domain that has a highly ordered aminoacidic structure and consequently a crystalline secondary structure (mainly β-sheets) [28]. Instead, the light chain has a less ordered secondary structure and its mainly in random configuration [28]. During the solubilization in *LiBr* of fibroin and the successive dialysis the β structures were denaturated then the successive dialysis allowed the elimination of the salt. The final product was a protein in water solution with random secondary structure [29]. The successive rapid cooling in liquid nitrogen and the freeze drying ensured the maintenance of the random structure also in the solid phase [10]. Both fluorophores were added to a solution obtained by dissolving silk

Preprints (www.preprints.org) | NOT PEER-REVIEWED | Posted: 6 May 2021 doi:10.20944/preprints202105.0077.v1

fibroin in formic acid. The subsequent solvent casting allowed the formation of stable silk films. In fact, formic acid allowed the transition of the secondary structure to the stable β form (physical crosslinking) [30,31]. This was useful to effectively entrap the fluorophore molecules in a dense structure suitable for occurrence of the energy transfer. FRET occurred between fibroin and PPO ant then between PPO and LV. Interestingly while exiting tryptophan and tyrosine inside fibroin at 290nm the PPO emission increased due to FRET in accordance with the increasing of its amount in percentage. The trend for the PPO-LV couple was in countertendency, the increase of the amount of LV decreased its emission (with an excitation at 290nm). This effect could be explain considering that the efficiency depends also on the distance between the acceptor-donor, and in a complex system as the one that we are studying, is not straightforward the solute is evenly dispersed in the matrix, particularly in case of silk fibroin where the light and the heavy chains domain has different affinities [28]. In fact, the heavy chain is mainly hydrophobic while the light chain is hydrophilic [28]. We hypothesize that a lower amount of LV ensured a better dispersion of LV and thus a lower distance from the PPO molecules and a higher efficiency of the PPO-LV couple. With this composition we prepared an electro-spun mat and compared it with the same mats produced by the bare fibroin and with fibroin and PPO. Interestingly, the only mats that gave a nice outcome by confocal microscopy was the one produced by the addition of both PPO and LV. On that mats we were able to perform a deeper morphological analysis using mild 405 nm laser power level, allowing to obtain resolute Z-stacks with 1.6 μm thickness confocal plane.

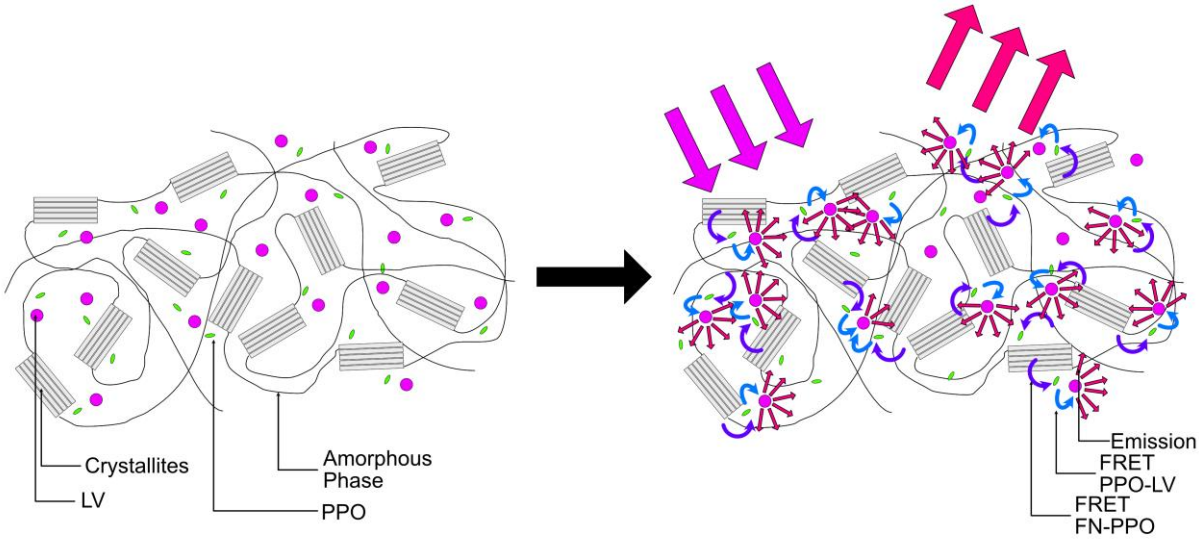

Figure 5. Structure of the produced samples and proposed mechanism of emission. The structure formed by solvent casting from formic acid was physically crosslinked due to the transition of the protein to the stable β-sheet structure. Both PPO and LV were entrapped inside the matrix. When the films were irradiated at the excitation wavelength of fibroin an energy transfer between fibroin and PPO occurred. A second energy transfer occurred between PPO and LV. The visible emission was then the one associated to LV.

5. Conclusion

In this work we demonstrated the possibility to use silk intrinsic fluorescence to image the morphology of silk fibroin construct. Using the fluorescent amino acids of fibroin in a donor-acceptor couple in which PPO was used as acceptor we able to suppress the fibroin intrinsic fluorescence transferring the energy to the PPO. With the addition of a second dye (LV) we were able to repeat the same donor-acceptor dynamics, which the result then when fibroin was exited the emission was due to LV. The energy transfer was confirmed by spectroscopy on fibroin films with the addition of one or both the fluorophores. The best composition of fibroin, PPO and LV was used to produce a fibroin electro spun mats that was observed by confocal microscopy to study its morphology. As results using FRET, we were able to effectively conduct a morphological analysis and quantify the fiber diameter distribution. This method could be potentially used to visu-

alized silk constructs whenever other methods are inconvenient. In addition, it could be applied to other protein or material with an intrinsic fluorescence.

Author Contributions: Alessio Bucciarelli wrote the manuscript, conceived the experiment, prepared part of the samples, collected and analyzed the data. Alberto Quaranta supervised the work and conceived the part related to the fluorescence, Devid Maniglio supervised the work prepared the silk fibroin mats collected and analyzed the confocal images. All the authors have edited the final version.

Data Availability Statement: The data is available from the author upon reasonable request.

Acknowledgments: In this section, you can acknowledge any support given which is not covered by the author contribution or funding sections. This may include administrative and technical support, or donations in kind (e.g., materials used for experiments).

Conflicts of Interest: The authors declare no conflict of interest.

References

1. Yang, Y.J.; Ganbat, D.; Aramwit, P.; Bucciarelli, A.; Chen, J.; Migliaresi, C.; Motta, A. Processing keratin from camel hair and cashmere with ionic liquids. *Express Polym. Lett.* **2019**, *13*, doi:10.3144/expresspolymlett.2019.10.
2. Sultankulov, B.; Berillo, D.; Sultankulova, K.; Tokay, T.; Saparov, A. Progress in the development of chitosan-based biomaterials for tissue engineering and regenerative medicine. *Biomolecules* 2019, *9*.
3. Sun, J.; Tan, H. Alginate-based biomaterials for regenerative medicine applications. *Materials (Basel).* 2013, *6*, 1285–1309.
4. Echave, M.C.; Burgo, L.S.; Pedraz, J.L.; Orive, G. Gelatin as Biomaterial for Tissue Engineering. *Curr. Pharm. Des.* **2017**, *23*, doi:10.2174/0929867324666170511123101.
5. Rockwood, D.N.; Preda, R.C.; Yücel, T.; Wang, X.; Lovett, M.L.; Kaplan, D.L. Materials fabrication from Bombyx mori silk fibroin. *Nat. Protoc.* **2011**, *6*, 1612–1631, doi:10.1038/nprot.2011.379.
6. Bucciarelli, A.; Greco, G.; Corridori, I.; Pugno, N.M.; Motta, A. A Design of Experiment Rational Optimization of the Degumming Process and Its Impact on the Silk Fibroin Properties. *ACS Biomater. Sci. Eng.* **2021**, acsbiomaterials.0c01657, doi:10.1021/acsbiomaterials.0c01657.
7. Hwi Cho, H.; Young Been, S.; Youp Kim, W.; Min Choi, J.; Hee Choi, J.; Ui Song, C.; Eun Song, J.; Bucciarelli, A.; Khang, G. Comparative Study on the Effect of the Different Harvesting Sources of Demineralized Bone Particles on the Bone Regeneration of a Composite Gellan Gum Scaffold for Bone Tissue Engineering Applications. *ACS Appl. Bio Mater.* **2021**, *0*, doi:10.1021/acsabm.0c01549.
8. Been, S.; Choi, J.; Cho, H.; Jeon, G.; Song, J.E.; Bucciarelli, A.; Khang, G. Preparation and characterization of a soluble eggshell membrane/agarose composite scaffold with possible applications in cartilage regeneration. *J. Tissue Eng. Regen. Med.* **2021**, term.3178, doi:10.1002/term.3178.
9. Bucciarelli, A.; Muthukumar, T.; Kim, J.S.; Kim, W.K.; Quaranta, A.; Maniglio, D.; Khang, G.; Motta, A. Preparation and Statistical Characterization of Tunable Porous Sponge Scaffolds using UV Cross-linking of Methacrylate-Modified Silk Fibroin. *ACS Biomater. Sci. Eng.* **2019**, *5*, 6374–6388, doi:10.1021/acsbiomaterials.9b00814.
10. Bucciarelli, A.; Chiera, S.; Quaranta, A.; Yadavalli, V.K.; Motta, A.; Maniglio, D. A Thermal-Reflow-Based Low-Temperature, High-Pressure Sintering of Lyophilized Silk Fibroin for the Fast Fabrication of Biosubstrates. *Adv. Funct. Mater.* **2019**, *29*, 1901134, doi:10.1002/adfm.201901134.
11. Cho, H.; Bucciarelli, A.; Kim, W.; Jeong, Y.; Kim, N.; Jung, J.; Yoon, S.; Khang, G. Natural Sources and Applications of Demineralized Bone Matrix in the Field of Bone and Cartilage Tissue Engineering. In *Bioinspired Biomaterials. Advances in Experimental Medicine and Biology*; Chun, H.J., Reis, R.L., A., M., Khang, G., Eds.; Springer, Singapore, 2020; pp. 3–14.
12. Zhu, B.; Wang, H.; Leow, W.R.; Cai, Y.; Loh, X.J.; Han, M.Y.; Chen, X. Silk Fibroin for Flexible Electronic Devices. *Adv.*

Mater. **2016**, *28*, 4250–4265, doi:10.1002/adma.201504276.

13. Bucciarelli, A.; Pal, R.K.; Maniglio, D.; Quaranta, A.; Mulloni, V.; Motta, A.; Yadavalli, V.K. Fabrication of Nanoscale Patternable Films of Silk Fibroin Using Benign Solvents. **2017**, *201700110*, 1–9, doi:10.1002/mame.201700110.
14. Bucciarelli, A.; Mulloni, V.; Maniglio, D.; Pal, R.K.; Yadavalli, V.K.; Motta, A.; Quaranta, A. A comparative study of the refractive index of silk protein thin films towards biomaterial based optical devices. *Opt. Mater. (Amst).* **2018**, *78*, 407–414, doi:10.1016/j.optmat.2018.02.058.
15. Lee, O.J.; Sultan, M.T.; Hong, H.; Lee, Y.J.; Lee, J.S.; Lee, H.; Kim, S.H.; Park, C.H. Recent Advances in Fluorescent Silk Fibroin. *Front. Mater.* 2020, *7*, 50.
16. Georgakoudi, I.; Tsai, I.; Greiner, C.; Wong, C.; Defelice, J.; Kaplan, D. Intrinsic fluorescence changes associated with the conformational state of silk fibroin in biomaterial matrices. *Opt. Express* **2007**, *15*, 1043–1053, doi:10.1364/OE.15.001043.
17. Amirikia, M.; Shariatzadeh, S.M.A.; Jorsaraei, S.G.A.; Mehranjani, M.S. Auto-fluorescence of a silk fibroin-based scaffold and its interference with fluorophores in labeled cells. *Eur. Biophys. J.* **2018**, *47*, 573–581, doi:10.1007/s00249-018-1279-1.
18. Hussain, S.A. An Introduction to Fluorescence Resonance Energy Transfer (FRET). *Energy* **2009**, *132*, 4.
19. Preus, S.; Wilhelmsson, L.M. Advances in Quantitative FRET-Based Methods for Studying Nucleic Acids. *ChemBioChem* **2012**, *13*, 1990–2001, doi:10.1002/cbic.201200400.
20. Sekar, R.B.; Periasamy, A. Fluorescence resonance energy transfer (FRET) microscopy imaging of live cell protein localizations. *J. Cell Biol.* **2003**, *160*, 629–633, doi:10.1083/jcb.200210140.
21. Li, H.; Huang, X.X.; Kong, D.M.; Shen, H.X.; Liu, Y. Ultrasensitive, high temperature and ionic strength variation-tolerant Cu2+ fluorescent sensor based on reconstructed Cu2+-dependent DNAzyme/substrate complex. *Biosens. Bioelectron.* **2013**, *42*, 225–228, doi:10.1016/j.bios.2012.10.070.
22. Jiang, W.; Yang, S.; Lu, W.; Gao, B.; Xu, L.; Sun, X.; Jiang, D.; Xu, H.-J.; Ma, M.; Cao, F. A novel fluorescence "turn off-on" nano-sensor for detecting Cu2+ and Cysteine in living cells. *J. Photochem. Photobiol. A Chem.* **2018**, *362*, 14–20, doi:10.1016/j.jphotochem.2018.05.004.
23. Danos, L.; Parel, T.; Markvart, T.; Barrioz, V.; Brooks, W.S.M.; Irvine, S.J.C. Increased efficiencies on CdTe solar cells via luminescence down-shifting with excitation energy transfer between dyes. *Sol. Energy Mater. Sol. Cells* **2012**, *98*, 486–490, doi:10.1016/j.solmat.2011.11.009.
24. Quaranta, A.; Carturan, S.; Marchi, T.; Cinausero, M.; Scian, C.; Kravchuk, V.L.; Degerlier, M.; Gramegna, F.; Poggi, M.; Maggioni, G. Doping of polysiloxane rubbers for the production of organic scintillators. In Proceedings of the Optical Materials; Elsevier B.V., 2010; Vol. 32, pp. 1317–1320.
25. Team, R.C. R: A Language and Environment for Statistical Computing. *Vienna, Austria* **2019**.
26. Plotly Technologies Inc. Collaborative data science Available online: https://plot.ly.
27. Schneider, C.A.; Rasband, W.S.; Eliceri, K.W. NIH Image to ImageJ: 25 years of image analysis. *Nat. Methods* **2012**, *9*, 671–675.
28. Koh, L.D.; Cheng, Y.; Teng, C.P.; Khin, Y.W.; Loh, X.J.; Tee, S.Y.; Low, M.; Ye, E.; Yu, H.D.; Zhang, Y.W.; et al. Structures, mechanical properties and applications of silk fibroin materials. *Prog. Polym. Sci.* **2015**, *46*, 86–110, doi:10.1016/j.progpolymsci.2015.02.001.
29. Wang, H.-Y.Y.; Zhang, Y.-Q.Q. Effect of regeneration of liquid silk fibroin on its structure and characterization. *Soft Matter* **2013**, *9*, 138–145, doi:10.1039/c2sm26945g.
30. Um, I.C.; Kweon, H.; Park, Y.H.; Hudson, S. Structural characteristics and properties of the regenerated silk fibroin prepared from formic acid. *Int. J. Biol. Macromol.* **2001**, *29*, 91–97, doi:10.1016/S0141-8130(01)00159-3.

 doi:10.20944/preprints202105.0077.v1

31. Um, I.C.; Kweon, H.Y.; Lee, K.G.; Park, Y.H. The role of formic acid in solution stability and crystallization of silk protein polymer. *Int. J. Biol. Macromol.* **2003**, *33*, 203–213, doi:10.1016/j.ijbiomac.2003.08.004.